ADVANCES IN ATMOSPHERIC SCIENCES, VOL. 25, NO. 1, 2008, 11–23

Total Deformation and its Role in Heavy Precipitation Events Associated with Deformation-Dominant Flow Patterns

GAO Shouting*[1] (高守亭), YANG Shuai[1,2] (杨 帅),
XUE Ming[3] (薛 明), and CUI Chunguang[4] (崔春光)

[1] *Laboratory of Cloud-Precipitation Physics and Severe Storms* (*LACS*),

Institute of Atmospheric Physics, Chinese Academy of Sciences, Beijing 100029

[2] *Graduate University of Chinese Academy of Sciences, Beijing* 100049

[3] *School of Meteorology and Center for Analysis and Prediction of Storms,*

University of Oklahoma, Norman Oklahoma, USA

[4] *Institute of Heavy Rain, China Meteorological Administration* (*CMA*), *Wuhan* 430074

(Received 29 August 2006; revised 23 January 2007)

ABSTRACT

In this paper, it is elucidated that the total deformation (TD), defined as the square root of the sum of squared stretching deformation and squared shearing deformation, is an invariant independent of the coordinate system used. An idealized flow field is then constructed to demonstrate the confluence effect of a non-divergent and irrotational deformation field on moisture transport. To explore the characteristics and role of TD, one heavy rainfall case that occurred in the middle and lower reaches of the Yangtze River (MRYR) over China, associated with a front with shear line, is analyzed using the Weather Research and Forecasting (WRF) model output data. It is found that right before the occurrence of precipitation, the effect of the confluence induced by deformation on moisture transport provides a favorable condition for precipitation.

During the precipitation, both location and orientation of the zone of large TD coincide with the confluent shear line. The rainbands are nearly parallel with, and located lightly to the south of the zones of large TD and the confluent shear line. The TD in the lower troposphere increases in value as precipitation persists. When TD approaches its maximal value, the next 6-hour precipitation reaches its peak correspondingly.

A tendency equation for TD is derived. The analysis of linear correlation and RMS difference between individual terms in the total deformation equation and the sum of the terms shows that the pressure gradient plays a major role in determining the local change of total deformation.

Key words: deformation, confluence, precipitation, equation

DOI: 10.1007/s00376-008-0011-y

1. Introduction

Among the basic variables that describe the atmosphere, namely, temperature, pressure, humidity and wind velocity, only wind velocity is a vector. At the mesoscale, where the characteristic scale is less than the Rossby radius of deformation, it is known that the wind field determines the mass field through geostrophic adjustment (Rossby, 1937, 1938; Yeh, 1957; Yeh and Li, 1982; Zeng, 1963a,b,c). At the even smaller, convective storm scale, the importance of wind field is even more evident. It is known that the environmental wind profile has a strong control on the storm types (Weisman and Klemp, 1982) and storm dynamics (e.g., Walter and Thorpe, 1979). The environmental helicity, defined as the dot product of the environmental velocity and vorticity vectors, plays an important role in the storm longevity and the ro-

*Corresponding author: GAO Shouting, gst@lasg.iap.ac.cn

tation characteristics of thunderstorms (e.g., Davies-Jones, 1984; Etling, 1985; Lilly, 1986a,b; Droegemeier et al., 1993; Lu and Gao, 2003).

The importance of the wind field has been recognized by many researchers. Petterssen (1956) showed that a 2D linear wind field could be expressed as a combination of translation, divergence, deformation, and vorticity components. Other researchers, including Wiin-Nielsen (1973) and Norbury (2002), have also discussed the above properties of wind fields in some detail. Traditionally, the divergence and vorticity are two quantities that have received most attention. The prognostic equations for vorticity and divergence derived from the equations of motion have been used extensively in the literature as well as in textbooks for studying dynamics of fluid flows and various atmospheric phenomena (Wu and Tan, 1989). The deformation has, in comparison, received much less attention except in studies of frontogenesis. For certain types of precipitation systems, such as those associated with the eastern China mei-yu front, the large-scale flow pattern often exhibits a dominant deformation pattern at the low levels while the divergence and vorticity are sometimes of smaller magnitudes. For these types of systems, it is important to understand the role of deformation, in the triggering and maintenance of the precipitation, and to gain insight on the time evolution of the deformation field.

In section 2 of this paper, an idealized flow model is first constructed to demonstrate the confluence effect of non-divergent and irrotational deformation on moisture. In section 3, it is shown that the total deformation is an invariant independent of the coordinate system used. A prognostic equation of the total horizontal deformation is derived. In section 4, one heavy rainfall case associated with a mei-yu front in an almost east-west orientation over eastern China is numerically simulated and analyzed. In section 5, the deformation field and its role associated with the heavy rainfall case are diagnosed and analyzed using the Weather Research and Forecasting (WRF) model output data. In section 6, the relative contributions to total deformation of the terms in the total deformation equation are analyzed for the rainfall case. Conclusions are given in section 7.

2. An idealized flow field model

A pure 2D deformation flow is non-divergent and irrotational. For this reason, it by itself does not produce vertical lifting at the low levels or create convergence through the Ekman pumping effect. But deformation is important in frontogenesis. It increases the horizontal temperature gradient, and therefore baroclinicity through advection, which also leads to frontogenesis. In addition, the deformation flow can play an important role in advecting moisture into a precipitation region.

To illustrate the role of a deformation-dominated flow field that is typical of the flow pattern associated with the mei-yu front, an idealized flow field of the typical "saddle" pattern is constructed. Our idealized flow field is constructed through a linear combination of two functions. Function 1 defines a vortex (Luther White, personal communication, 2006)

$$V_{\mathrm{T}}(R) = V_0 \left(\frac{\Phi_1 + \Phi_2}{2} \right) ,$$

where

$$\Phi_n(R, R_0) = \frac{2nR_0^{2n-1}R}{(2n-1)R_0^{2n} + R^{2n}} , \quad n = 1, 2, \ldots$$

This vortex contains two free parameters, n and R_0, where n is an integer, R_0 is a characteristic radius, and R the radius from the vortex center. This vortex looks like a smoothed version of the Rankine combined vortex (Harasti and List, 2005); in particular, it avoids the singularity point associated with the Rankine combined vortex at $R = R_0$ (Fig. 1).

Note that, here, V_{T} is the tangential wind speed with the vortex, V_0 the maximum value of V_{T} at radius R_0, and R is the radius for the constructed high and low circulations.

And function 2 specifies a pure deformation flow:

$$\begin{cases} u = bx , \\ v = -by , \end{cases}$$

where b is a positive constant. A linear combination

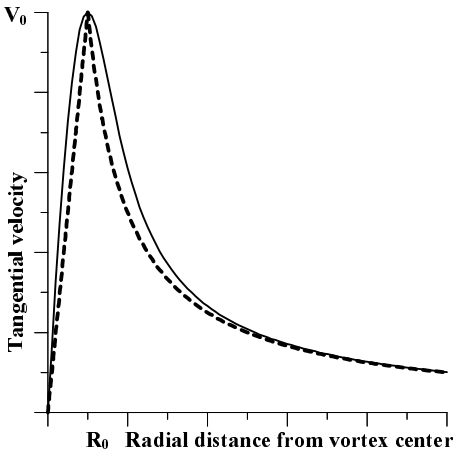

Fig. 1. Tangential velocity derived from the traditional Rankine combined vortex (solid line) and vortex (dashed line), which looks like a smoothed version of the Rankine combined vortex.

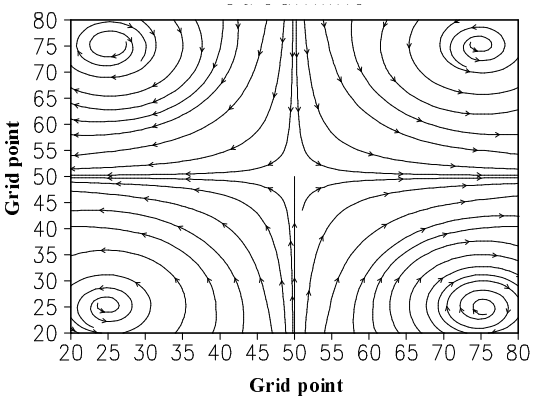

Fig. 2. Constructed idealized flow field with two highs and two lows.

of them gives

$$\begin{pmatrix} u \\ v \end{pmatrix} = \alpha K(m) V_{\mathrm{T}}(R) \begin{pmatrix} -\sin\theta \\ \cos\theta \end{pmatrix} + (1-\alpha) \begin{pmatrix} bx \\ -by \end{pmatrix} , \quad (1)$$

where

$$K(m) = \begin{cases} 1, & \text{when } m = 1 \text{ or } 3 \\ -1, & \text{when } m = 2 \text{ or } 4 \end{cases} ,$$

where $m = 1, 2, 3, 4$ denote the No. m quadrant;

$$\tan\theta = \frac{y - Y_{0m}}{x - X_{0m}} , \quad \sin\theta = \frac{y - Y_{0m}}{R} ,$$

$$\cos\theta = \frac{x - X_{0m}}{R} , \quad x = (i - 51)\Delta x ,$$

$$y = (j - 51)\Delta y ,$$

where the total grid points are 101×101,

$$R = R(x, y) = \sqrt{(x - X_{0m})^2 + (y - Y_{0m})^2} .$$

$$(X_{0m}, Y_{0m}) =$$

$$\begin{cases} (X_{01}, Y_{01}) = (25\Delta x, 25\Delta y) & \text{when } m = 1 \\ (X_{02}, Y_{02}) = (-25\Delta x, 25\Delta y) & \text{when } m = 2 \\ (X_{03}, Y_{03}) = (-25\Delta x, -25\Delta y) & \text{when } m = 3 \\ (X_{04}, Y_{04}) = (25\Delta x, -25\Delta y) & \text{when } m = 4 \end{cases}$$

are the four centers of constructed high and low circulations. The deformation coefficient $b = 1.6 \times 10^{-5}$. The center of the flow region is at the origin of the coordinate system. The velocity is calculated on a 101×101-grid at a grid spacing of 60 km (i.e., we take $\Delta x = \Delta y = 60$ km). In Eq. (1), α is a weight determined by

$$\alpha = \begin{cases} 0 , & R_{i,j} > R_0 \\ \dfrac{R_{i,j}}{25\Delta x} , & R_1 < R_{i,j} \leqslant R_0 \\ 1 , & 0 < R_{i,j} \leqslant R_1 \end{cases}$$

where Δx is the grid spacing. $R_0 = 1200$ km, $R_1 = 900$ km.

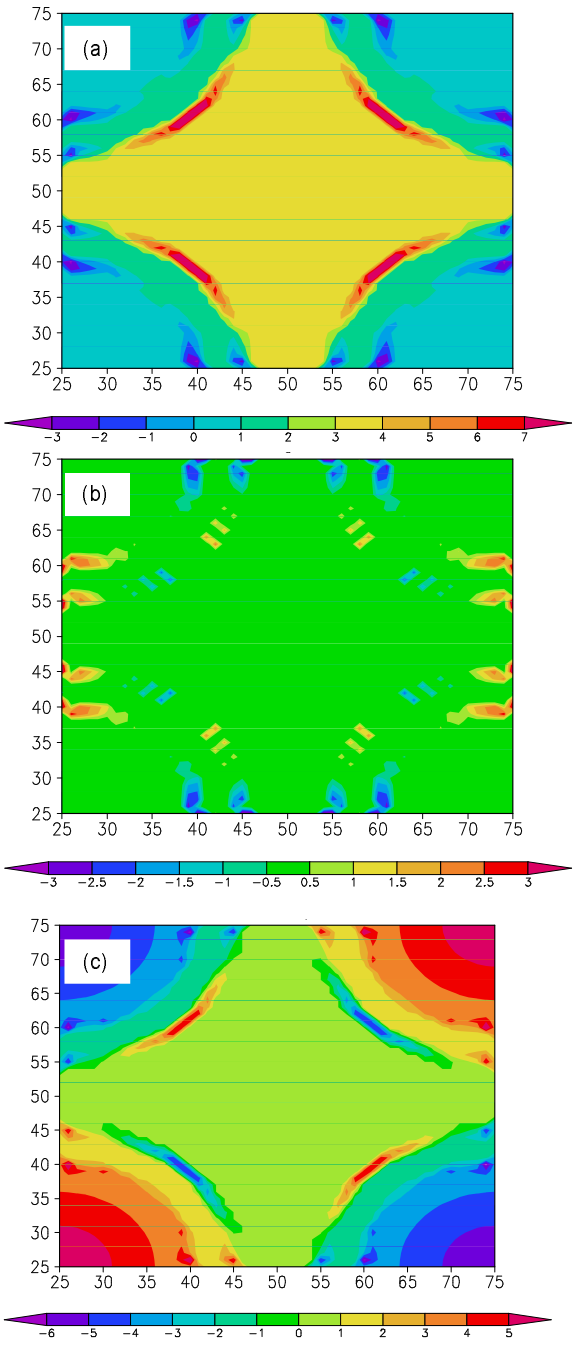

Fig. 3. (a) Deformation, (b) divergence and (c) vorticity fields (10^{-5} s^{-1}) of the idealized flow shown in Fig. 1.

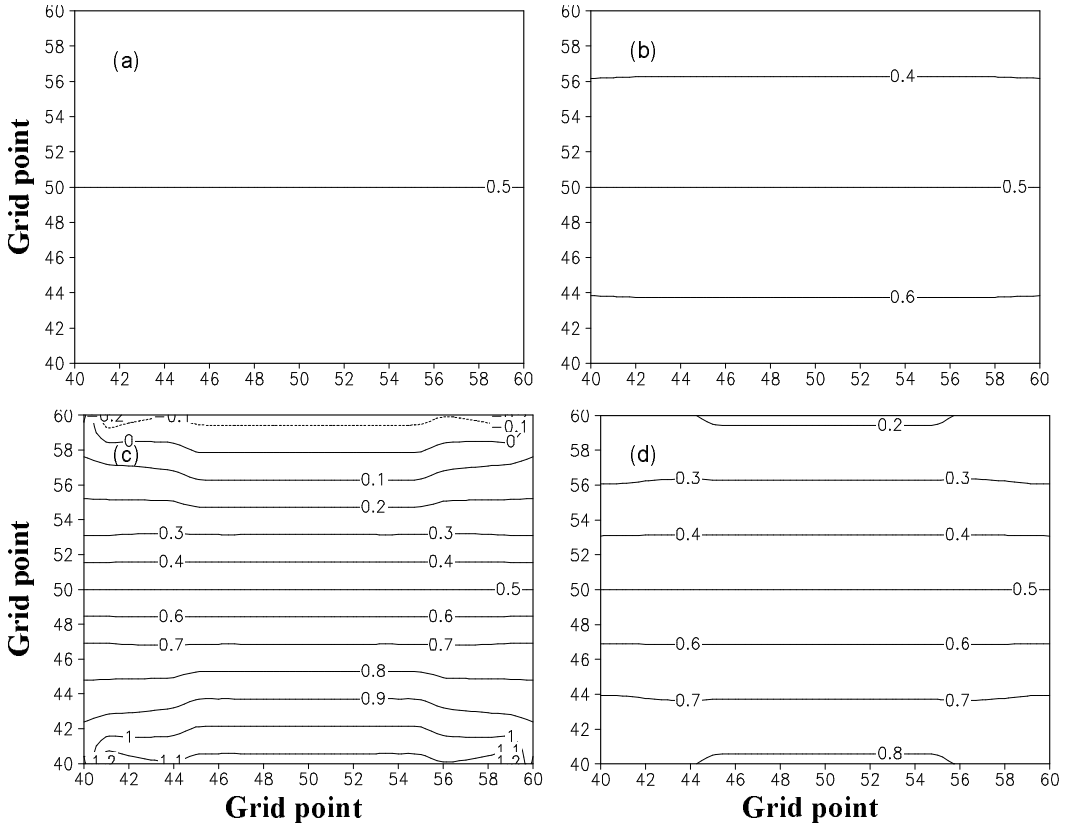

Fig. 4. A 2D relative humidity field subjecting to the advection by the idealized deformation flow field, at (a) 0 hour, (b) 12 hours, (c) 24 hours and (d) 36 hours. The contour intervals are 0.1, and all contours at time zero have an east-west orientation.

This idealized flow (Fig. 2) consists of two highs (anticyclones) and two lows (cyclones) and an east-west confluence zone exists between the high-low couplets to the north and the low-high couplets to the south. In the confluence zone, both vorticity and divergence are actually small or zero while deformation is large (Fig. 3). The value of deformation is 3.2×10^{-5} in the middle part of the domain (region with orange shading in Fig. 3a), while both divergence and vorticity are zero in this region (Figs. 3b and 3c). Note that the two rings of blue and orange in the divergence field are the results of the truncation errors in the finite difference calculation and the discontinuity between the regions where the flows are defined by different functions. The same reason leads to the two rings in vorticity and deformation fields.

For typical mei-yu frontal systems, the horizontal temperature gradient is usually weak, and therefore the classical frontogensis processes associated with deformation flow are less important. An uniform background potential temperature and an initial background relative moisture field (noted as q) are assumed as functions of y. And q is specified as $q = 0.9 - 0.008(y - 1)$, where y is the grid index in the y direction. Subject to the advection of this flow, the isolines of relative humidity after 6 hours are concentrated distinctly towards the confluence region of the "saddle" field, while the isolines after 12 hours become even denser (Fig. 4b). After 36 hours, the isolines become much more concentrated (Fig. 4d), indicating a buildup of strong moisture gradient along the confluence zone. In the case of three dimensions, vertical motion along the confluence zone will cause the upward transport of the moisture brought in by the horizontal deformation flow.

Often, the moisture gradient zone is not parallel to the confluence zone. An example of such is when the initial relative humidity (q) is specified by $q = 0.9+0.008(x-y)$, where x is the grid index in the x direction. Figure 5 shows the evolution of this humidity field subject to the advection of the same idealized flow. The contours of relative humidity also become more concentrated as in the previous case; moreover, the orientations of these contours become more and more parallel to the confluence zone (Fig. 5). Eventually, the zone of strong moisture gradient becomes parallel to the confluence zone.

In the real atmosphere, this type of "saddle" flow

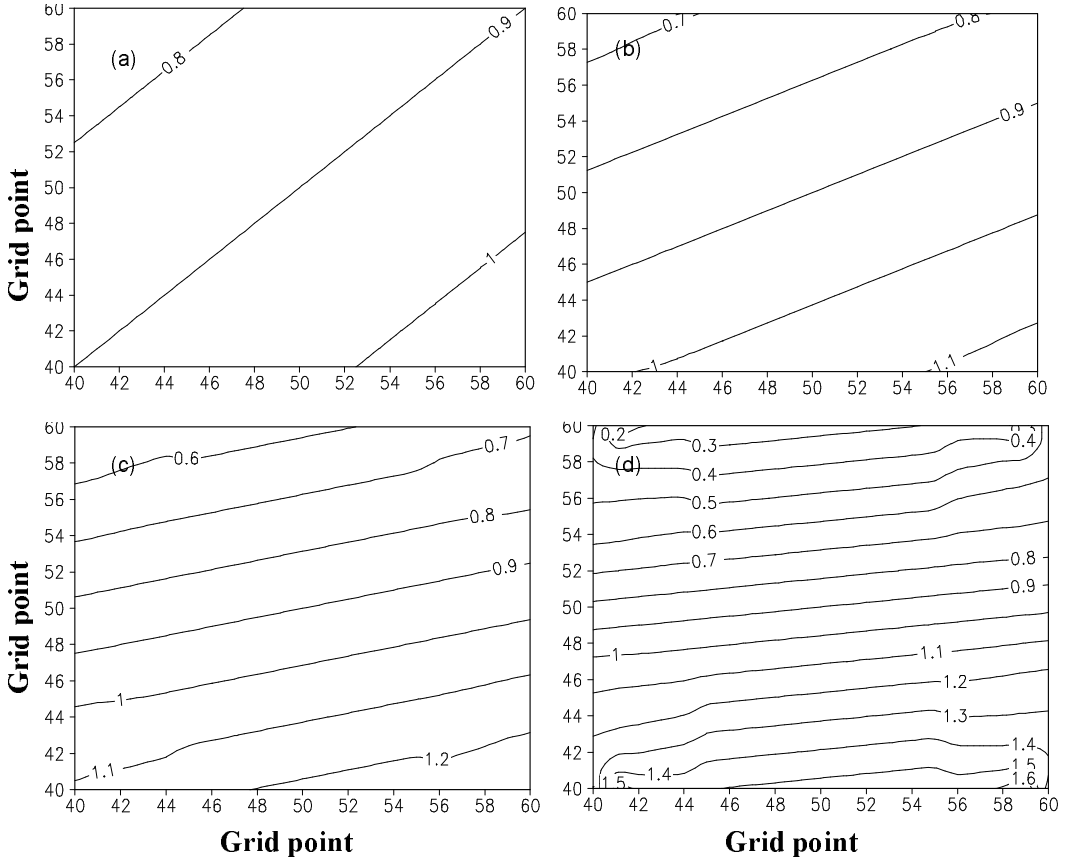

Fig. 5. A 2D relative humidity field subjecting to the advection by the idealized deformation flow field, at (a) 0 hour, (b) 12 hours, (c) after 24 hours and (d) 36 hours. The contour intervals are 0.1 and all contours at time zero have a southwest-northeast orientation.

is often found. Moreover, it is often associated with precipitation. Since the vorticity and divergence are small in such a flow while the deformation is large, even in the absence of a distinct temperature gradient, heavy precipitation can result from the confluence associated with the deformation, through the focusing effect on moisture. The richness of moisture in the confluence zone provides a favorable condition for moist convection, although the actual triggering of convection is usually provided by something else, such as upper-level lifting by a short-wave trough, or weak but still present low-level convergence (Hoxit et al., 1978; Maddox et al., 1978; Caracena et al., 1979; Maddox et al., 1980a,b). These will be discussed in detail for two real precipitation cases in sections 4 and 5.

3. Total deformation and its prediction equation

3.1 *Total deformation*

In Petterssen (1956), it is shown that a two-dimensional velocity field, (u, v), can be approximated by a truncated Taylor series,

$$u = u_0 + (D + F)x/2 - (r - q)y/2 \,, \qquad (2a)$$

$$v = v_0 + (r + q)x/2 + (D - F)y/2 \,, \qquad (2b)$$

where u_0 and v_0 are velocity components at the coordinate origin, and

$$D = \left(\frac{\partial u}{\partial x} + \frac{\partial v}{\partial y}\right) \,, \quad q = \left(\frac{\partial v}{\partial x} - \frac{\partial u}{\partial y}\right) \,,$$

$$F = \left(\frac{\partial u}{\partial x} - \frac{\partial v}{\partial y}\right) \,, \text{ and } \quad r = \left(\frac{\partial v}{\partial x} + \frac{\partial u}{\partial y}\right) \,,$$

which are, respectively, the divergence, vorticity, stretching deformation, and shearing deformation. The equation shows that a 2D flow can be locally expressed as a linear combination of the above four quantities.

Total deformation is usually defined as $E = \sqrt{F^2 + r^2}$ (Petterssen, 1956; Keyser et al., 1986, 1988; Norbury, 2002). We show in the following that the magnitude of total deformation is independent of the coordinate used, the same as the divergence and vorticity.

We rotate the (x, y) coordinate system anticlockwise by angle θ, into a new coordinate system (x', y'). The coordinate transform relations are and $x' = x\cos\theta + y\sin\theta$ and $y' = y\cos\theta - x\sin\theta$. Therefore, it can be shown that

$$\begin{aligned} F &= \frac{\partial u}{\partial x} - \frac{\partial v}{\partial y} \\ &= \left(\frac{\partial u'}{\partial x'} - \frac{\partial v'}{\partial y'}\right)\cos 2\theta - \left(\frac{\partial v'}{\partial x'} + \frac{\partial u'}{\partial y'}\right)\sin 2\theta \\ &= F'\cos(2\theta) - r'\sin(2\theta) \end{aligned} \tag{3a}$$

$$\begin{aligned} r &= \frac{\partial v}{\partial x} + \frac{\partial u}{\partial y} \\ &= \left(\frac{\partial u'}{\partial x'} - \frac{\partial v'}{\partial y'}\right)\sin 2\theta + \left(\frac{\partial v'}{\partial x'} + \frac{\partial u'}{\partial y'}\right)\cos 2\theta \\ &= F'\sin(2\theta) + r'\cos(2\theta) \end{aligned} \tag{3b}$$

Therefore, $E^2 = F^2 + r^2 = F'^2 + r'^2$, where prime denotes the quantity in the rotated coordinate. This says that the magnitude of total deformation is independent of the coordinate system. For this reason, the total deformation is a more meaningful quantity to analyze than the individual components of the deformation, and it will be the primary quantity we examine in this paper. In the next subsection, we will derive the total deformation equation.

3.2 *Total deformation equation*

The horizontal equations of motion in the p-coordinate are

$$\begin{aligned} &\frac{\partial u}{\partial t} + u\frac{\partial u}{\partial x} + v\frac{\partial u}{\partial y} + \omega\frac{\partial u}{\partial p} - fv = \\ &\quad -g\frac{\partial z}{\partial x} + F_x\,, \end{aligned} \tag{4a}$$

$$\begin{aligned} &\frac{\partial v}{\partial t} + u\frac{\partial v}{\partial x} + v\frac{\partial v}{\partial y} + \omega\frac{\partial v}{\partial p} + fu = \\ &\quad -g\frac{\partial z}{\partial y} + F_y\,. \end{aligned} \tag{4b}$$

By the operation of

$$\begin{aligned} &\frac{F}{\sqrt{F^2+r^2}}\left[\frac{\partial}{\partial x}(4a) - \frac{\partial}{\partial y}(4b)\right] + \\ &\frac{r}{\sqrt{F^2+r^2}}\left[\frac{\partial}{\partial y}(4a) + \frac{\partial}{\partial x}(4b)\right]\,, \end{aligned}$$

we obtain the equation for total deformation, E,

$$\frac{\partial E}{\partial t} = \text{term1}+\text{term2}+\text{term3}+\text{term4}+\text{term5}+\text{term6}\,, \tag{5a}$$

where

$$\text{term1} = -\boldsymbol{V}\cdot\nabla E\,, \tag{5b}$$

$$\text{term2} = -E\nabla_{\mathrm{h}}\cdot\boldsymbol{V} \tag{5c}$$

$$\text{term3} = \frac{uF+vr}{E}\frac{\partial f}{\partial y}\,, \tag{5d}$$

$$\text{term4} = -\frac{F}{E}\left(g\frac{\partial^2 z}{\partial x^2} - g\frac{\partial^2 z}{\partial y^2}\right) - \frac{r}{E}\left(2g\frac{\partial^2 z}{\partial x\partial y}\right)\,, \tag{5e}$$

$$\begin{aligned} \text{term5} = &\frac{F}{E}\left(\frac{\partial\omega}{\partial x}\frac{\partial u}{\partial p} - \frac{\partial\omega}{\partial y}\frac{\partial v}{\partial p}\right) + \\ &\frac{r}{E}\left(\frac{\partial\omega}{\partial y}\frac{\partial u}{\partial p} + \frac{\partial\omega}{\partial x}\frac{\partial v}{\partial p}\right)\,, \end{aligned} \tag{5f}$$

$$\text{term6} = \frac{F}{E}\left(\frac{\partial F_x}{\partial x} - \frac{\partial F_y}{\partial y}\right) + \frac{r}{E}\left(\frac{\partial F_x}{\partial y} + \frac{\partial F_y}{\partial x}\right)\,. \tag{5g}$$

Here, $\boldsymbol{V}$ is the 3D wind vector and $\nabla_{\mathrm{h}}\cdot\boldsymbol{V}$ is the horizontal divergence and $\omega = dp/dt$ is the vertical velocity in pressure coordinate. From Eq. (5a), we can see that the local change of total deformation is caused by advection (term1), horizontal divergence (term2), the term related to β-effect (term3), the pressure gradient term (term4), the vertical velocity contributions (term5), and the term related to frictional force and/or turbulence mixing (term6).

3.3 *The physical meaning of each term*

For the convenience of discussion, we can choose our coordinate so that the shearing deformation is zero. We consider a pure stretching deformation field defined by $u = \alpha x$ and $v = -\alpha y$. The flow described by this set of equations in the region close to the coordinate origin is the typical flow pattern associated with a two-high and two-low arrangement (see Fig. 2). For this flow, $\partial u/\partial x > 0$ and $\partial v/\partial y < 0$, and in the first quadrant $u > 0$ and $v < 0$.

Term1 in Eq. (5a) represents the advection of total deformation. The sign of this term $(-\boldsymbol{V}\cdot\nabla E)$ is determined by the angle between the velocity vector and the gradient of total deformation. When the angle is less than 90°, the projection of $\boldsymbol{V}$ on $-\nabla E$ is positive, so term1 is positive; otherwise, the term is negative.

Term2 represents the change in total deformation due to horizontal divergence. For a pure deformation field, $V_{\rm h} \cdot \boldsymbol{V} = 0$, so this term is zero.

Term3 is a term that is related to the β-effect or the longitudinal gradient of Coriolis parameter f. Its sign is determined by the interaction between u and $\partial f/\partial y$ under the new coordinate (which makes $r = 0$) system.

Term4 represents the effect of pressure force. Under the assumption of a pure stretching deformation flow pattern, it can be rewritten as

$$-\left(g\frac{\partial^2 z}{\partial x^2} - g\frac{\partial^2 z}{\partial y^2}\right) .$$

Its contribution to the total deformation is determined by the combination of the shear in the x and y directions of pressure force (x and y represent the new coordinate axis under which the shear deformation is zero.).

Term5 combines the horizontal shear of vertical velocity with the vertical shear of horizontal velocity in the new coordinate system. Under the above assumption ($r = 0$), term5 can be rewritten as

$$\frac{\partial\omega}{\partial x}\frac{\partial u}{\partial p} - \frac{\partial\omega}{\partial y}\frac{\partial v}{\partial p} .$$

Its contribution to the change of total deformation is determined by the interaction of signs of the components.

4. Analysis of the rainfall case in July 2003 over China

The role of vorticity and divergence during the occurrence and development of torrential rain events has been investigated extensively in the literature (e.g. Herbert, 1954; Stanley and Michael, 1978a,b; Liebmann et al., 1998; Davidson et al., 1998; David and Anderson, 2001), but the role of total deformation before the occurrence and during the course of heavy rainfall has received much less attention. Bluestein (1977) studied the synoptic-scale deformation related to tropical cloud bands. Significant correlations were found between the cloud bands and the orientation of the axis of dilatation of objectively analyzed nondivergent winds at the lower troposphere. But studies on the correlations between deformation and precipitation are few. For this reason, one heavy rainfall case associated with the East China front is selected to explore the characteristics and role of total deformation before and during the rainfall events. The orientation of the rain band was almost east-west in the rainfall case.

A heavy rainfall event associated with a mei-yu front occurred in the middle and lower reaches of the Yangtze River (MRYR) over China from 0000 UTC 4 July to 1200 UTC 5 July 2003. The rainband was oriented in the west-southwest to east-northeast direction. The mei-yu front formed before the onset of precipitation and was maintained during the course of precipitation.

Figure 6a shows that at the 700-hPa level, there is a zone of high equivalent potential temperature, θ_e, that clearly marks the mei-yu frontal zone that stretches in the northeast-southwest orientation between 27°N and 36°N. Along this zone, especially near the northern edge of this zone, a line of strong confluence exists that is also a shear zone (Fig. 6b). This confluent shear zone is a result of the large-scale flow pattern that consists of a subtropical high located in the northwestern Pacific, a mid-to-high latitude low centered to the north at 48°N and 126°E, and a general anticyclonic flow pattern over much of China north of the Yantze River. This flow pattern differs from the classical "saddle" type deformation pattern for the lack of another low to the southwest and the oversize of the subtropical high. The result of this is the existence of a significant amount of shear or vorticity along the confluence zone. At the 200-hPa level, the precipitation region is dominated by a divergence flow along the northeast edge of the South Asia high (not shown). Therefore, the low-level confluence associated with the deformation flow pattern and the upper-level divergence set up a favorable circulation pattern for heavy mei-yu precipitation.

In order to obtain data at higher spatial and temporal resolutions for the above case and to use the data for a diagnostic study, we performed a numerical simulation using the Advanced Research WRF model, initializing the model using the archived $1° \times 1°$ NCEP/NCAR (National Center for Environmental Prediction/National Centers for Atmospheric Research) real-time global analyses data. The Advanced Research WRF (ARW) dynamic core uses compressible, non-hydrostatic equations. It uses the 3rd-order Runge-Kutta time-integration scheme (Wicker and William, 2002). For our simulations, the physics options used include the Ferrier microphysics scheme and the Kain-Fritsch cumulus parameterization scheme (Kain and Fritsch, 1990), the Medium-Range Forecast (MRF) boundary scheme (Hong and Pan, 1996), Dudhia shortwave radiation (Dudhia, 1989), as well as the Rapid Radiative Transfer Model (RRTM) longwave radiation scheme (Mlawer et al., 1997). The NCEP analyses at 6-hour intervals are used as the boundary conditions. The center of the 27-km resolution model domain is at 32°N and 117°E and has 181×161 grids in the horizontal and 31 non-uniformly-spaced terrain-following levels in the ver-

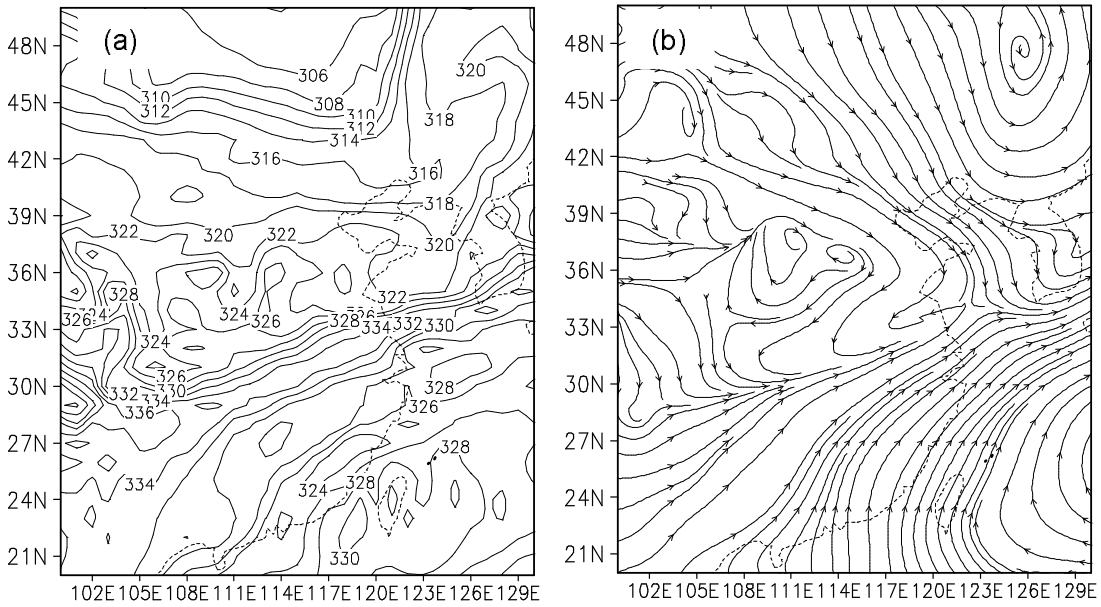

Fig. 6. The (a) equivalent potential temperature (K) and (b) streamline fields at the 700-hPa level at 0000 UTC 4 July 2003.

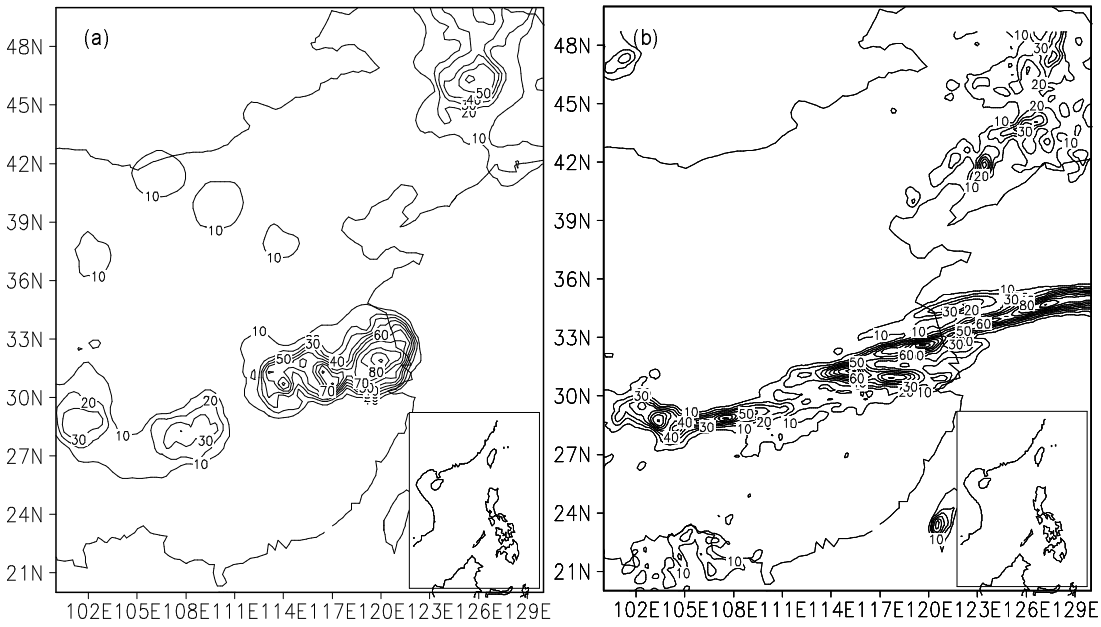

Fig. 7. (a) Observed and (b) simulated 36-hour cumulative rainfall (mm) over the middle and lower reaches of the Yangtze River from 0000 UTC 4 July to 1200 UTC 5 July 2003.

tical. The large time step used is 120 s. The 36-hour integration starts at 0000 UTC 4 July 2003 and output at 20-minute intervals are saved. Figures 7a and 7b show the observed and simulated 36-hour cumulative precipitation between 0000 UTC 4 July and 1200 UTC 5 July 2003. The simulated and observed maximum precipitation centers in MRYR are located, respectively, at 32.5°N and 119.5°E and at 32°N and 120°E. The simulated rainfall amount is similar to the observed rainfall amount [both are about 110 mm $(36\ \mathrm{h})^{-1}$]. Due to a lack of observational data over the ocean, the simulated precipitation cannot be validated there. Nor are there any precipitation data over the Korean peninsula either. Otherwise, the general precipitation patterns along the Yangtze River match rather well. Thus, the simulated data will be used for

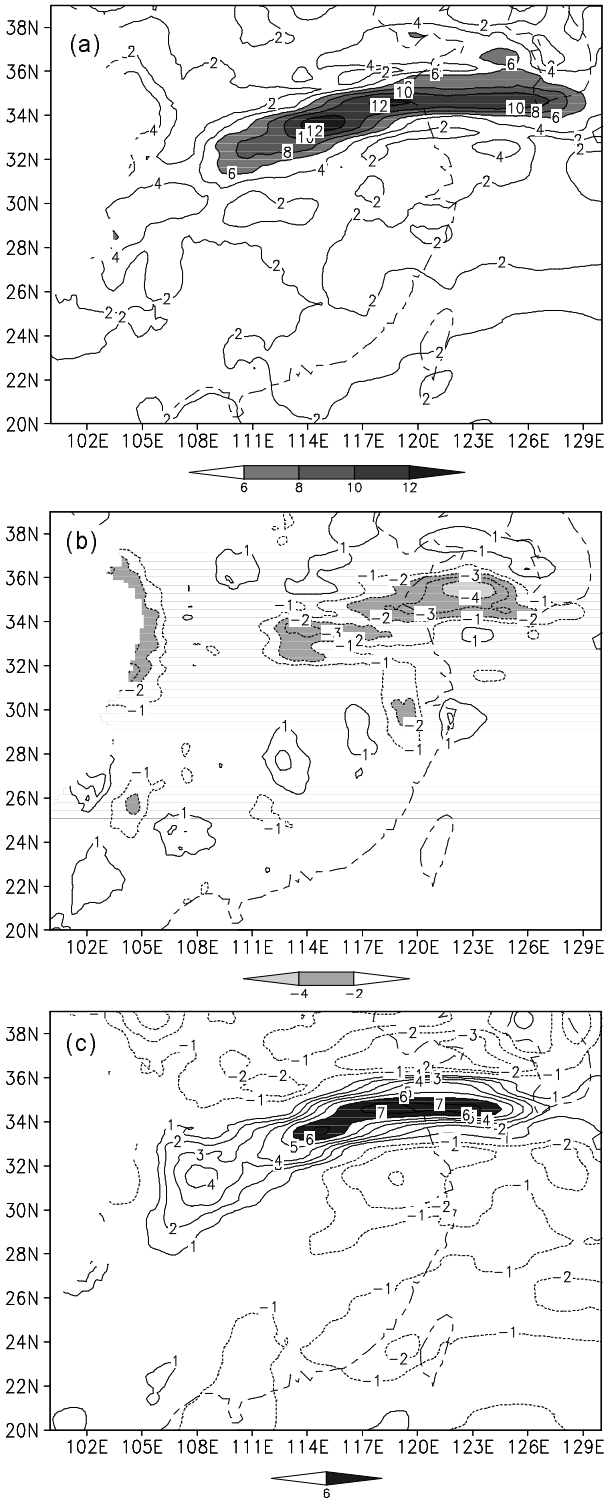

Fig. 8. (a) Total deformation, (b) divergence and (c) vorticity (10^{-5} s^{-1}) at the 700-hPa level at 0000 UTC 4 July 2003. The shaded areas represent values exceeding 6, −2 and 6, respectively, for the plotted fields.

diagnostic analysis.

5. Diagnostic analyses of total deformation and its relationship with precipitation

To examine the possible prognostic value of the total deformation field, as compared to the divergence and vorticity fields, these three fields are plotted in Fig. 8 at 700 hPa at 0000 UTC 4 July 2003, before the onset of precipitation. It can be seen from the figure that all the three fields show large values along a zone that more or less coincides with the band of the later 6-hour precipitation. The magnitude of absolute divergence is the smallest, with the maximum value being around 4×10^{-5} s^{-1}, while that of deformation is the largest, exceeding 1×10^{-4} s^{-1}. The vorticity maximum is about 7×10^{-5} s^{-1}. This shows quantitatively for such typical flow patterns associated with mei-yu fronts that total deformation is a dominant property of the flow, more so than convergence and vorticity. It is known that convergence and vorticity both have important roles to play in precipitation systems, by producing ascent via low-level convergence forcing, and by inducing low-level convergence via the Ekman pumping effect, respectively. Pure deformation contains no divergence or vorticity, but when it is the dominant property of the low-level flow, its effect cannot be overlooked. In this case, it plays an important role in low-level moisture transport, by bringing in moist air from the south side of the main confluence zone. This situation is similar to that of idealized deformation flow and the associated humidity advection considered in section 2.

Unlike classical cold or warm fronts, the horizontal temperature gradient associated with the mei-yu fronts is not strong—this can be seen from Fig. 9a for the current case. But the gradient of moisture is strong across the front and in the frontal zone (Fig. 9b). The zone of high relatively humidity at the 700-hPa level is a result of the lifting of moisture by the low-level confluent flow which also transports moisture horizontally into the zone, and the horizontal flow is dominated by the deformation. The results of this case show that the confluence associated with the total deformation focuses the moisture into the confluence zone, which provides a favorable condition for moisture convection. The convergence, though weaker relative to deformation, is still the one that triggers the convection via vertical lifting, but the role of deformation in the moisture transport is also important. Since large values of total deformation are present before the onset of precipitation, it is believed to have significant sense to the prognosis of precipitation.

After 0000 UTC 4 July 2003, precipitation began to occur and the rainband formed (Fig. 10) within the zone of large total deformation (Fig. 11). During the

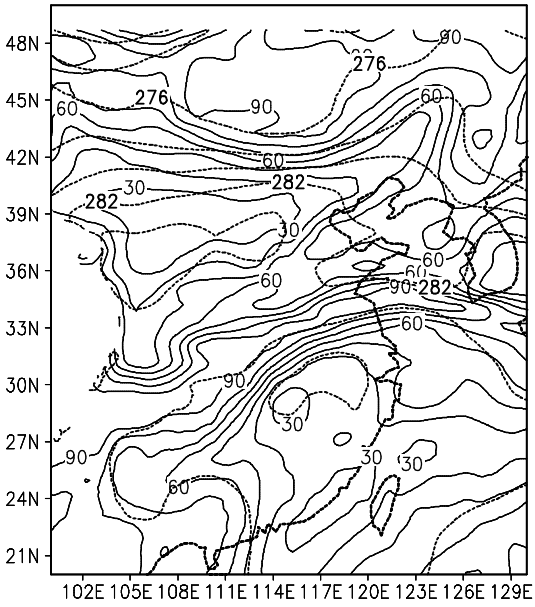

Fig. 9. Temperature (K, dashed line) and relatively humidity (%, solid line) at the 700-hPa level at 0000 UTC 4 July 2003.

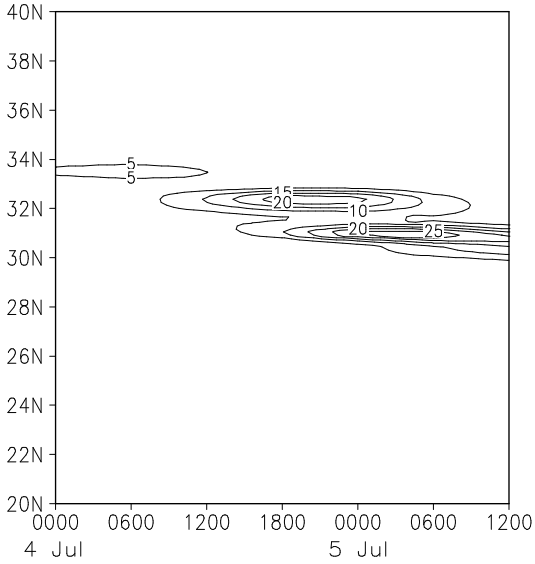

Fig. 10. Time-latitude cross section of 6-hour cumulative precipitation (mm) along 118°E from 0000 UTC 4 July to 1200 UTC 5 July 2003.

course of precipitation, the total deformation maximum is located slightly north of the maximum precipitation. Their trends are consistent with each other and both propagate southward from north of 33°N to 30°N. Two precipitation bands of more than 22 mm occur between 1700 UTC 4 July and 0000 UTC 5 July, and between 2300 UTC 4 July and 0800 UTC 5 July, respectively. A major band of large total deformation extends from 33°N at 1800 UTC 4 July to 31.5°N at 2100 UTC 4 July, and there is a slight increase in the total deformation during this period. Comparing Fig. 10 and Fig. 11, one can see that the large value of total deformation precedes the 6-hour cumulative precipitation maxima by 6 to 12 hours. The 6-hour precipitation reaches its maximum of 30 mm $(6h)^{-1}$ at 0600 UTC July 5 (Fig. 12a) whereas the 6-hour mean total deformation (Fig. 12b) reaches its peak magnitude of about 1.35×10^{-4} s^{-1} at 0000 UTC 5 July, 6 hours ahead of the precipitation maximum. The above analysis indicates that the total deformation has a predictive value for the precipitation more than 6 hours into the future.

Based on the above analyses on the rainfall case, some conclusions are drawn as follows. Before and during the course of precipitation, both the location and stretching directions of the band of large total deformation and of the confluent shear line overlap in the lower troposphere. The rainbands are located slightly to their southwest and the stretching direction of the rainband is generally the same as the large-value zone of deformation. The value of total deformation in the lower troposphere increases before the precipitation reaches its maximum intensity, and the time lag of the latter is often more than 6 hours. The magnitudes of both low-level divergence and vorticity are smaller than that of total deformation for the two typical precipitation cases examined, suggesting that the total deformation is at least an important precursor of heavy precipitation of the type analyzed here.

6. The relative contributions of the terms in the deformation equation

In the previous section, we analyzed the low-level deformation fields for the heavy rainfall case that occurred over China, and discussed the location and orientation relative to the confluence zone and the bands of strong vorticity and divergence. For the case, the deformation is found to have larger absolute magnitudes than either divergence or vorticity. The importance of the deformation field in these systems is evident. Further, in section 3, we derived the total deformation equation. In this section, using the WRF model output, we calculate the right-hand-side terms of the total deformation equation Eq. (5a), except for the friction term, for the rainfall case, in order to gain a better understanding of the processes contributing to the time evolution of total deformation.

For the July 2003 case, since the largest precipitation appears in the region of 30°–33°N and 114°–120°E (Figs. 7a and 7b), this region is chosen to calculate the

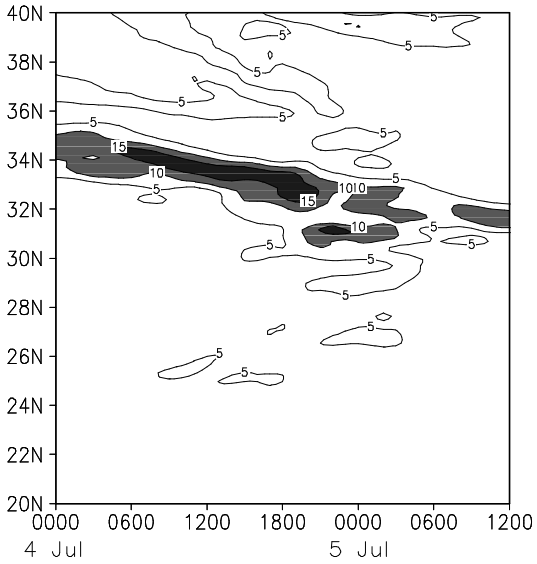

Fig. 11. Time-latitude cross section of total deformation (10^{-5} s^{-1}) along 118°E at the 700-hPa level from 0000 UTC 4 July to 1200 UTC 5 July 2003. The regions with total deformation exceeding 1×10^{-4} s^{-1} are shaded.

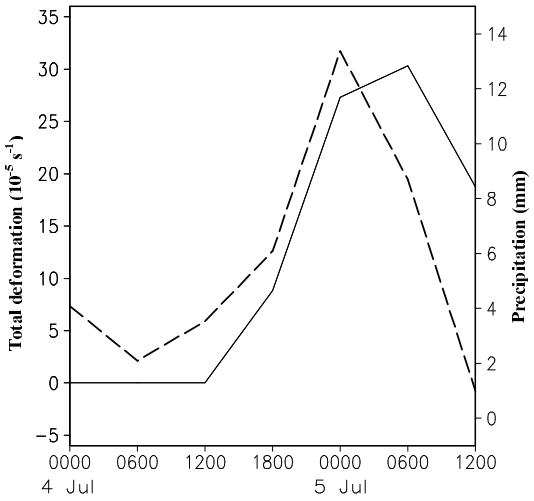

Fig. 12. Time series of 6-hour maximum cumulative precipitation (mm, solid line) and the magnitude of 6-hour time-mean total deformation (10^{-5} s^{-1}, dashed line) at 700 hPa at the center of precipitation at 32°N, 119°E from 0000 UTC 4 to 1200 UTC 5 July 2003.

area-mean of the terms in Eq. (5a) and the time tendency (Sum=Term1 + Term2+$\cdots\cdots$+Term5) from 0000 UTC 4 July to 1200 UTC 5 July 2003. The time series of these terms are plotted (not shown here). To identify the major processes that are responsible for the tendency of total deformation, the linear correlation coefficients and RMS differences between the sum and Terms 1 through 5 are calculated and presented in Table 1. It can be seen that Term2 has a negative correlation coefficient with the Sum whereas other terms have positive correlations. Term4 has the largest positive correlation coefficient of 0.979, and the smallest RMS difference of 5.1×10^{-10} s^{-2} among all terms. Term1 and Term5 have moderate positive correlation coefficients (around 0.5) and small RMS differences ($\sim$2.3–3.0$\times10^{-8}$ s^{-2}).

The above analysis indicates that the pressure gradient term is a major contributor to the local change of total deformation, whereas the vertical velocity term and the advection term also have considerable contributions. Since the effect of the pressure gradient term is dominant, in the deformation-dominant flow pattern where the high-low and low-high respectively couplet to both sides of the confluence zone, the pressure gradient is not only a force to trigger and maintain this kind of flow pattern, but it accelerates the deformation flow. Moreover, the focus of mass field towards the confluent zone, caused by the advection of deformation flow, has some positive feedback to the pressure gradient between both sides of the confluence zone. Therefore, the pressure gradient force has close relation to the change of local deformation. It is the basic and the dominant factor inducing the change of deformation-dominant flow patterns. Also due to the deformation-dominant flow pattern, the divergence is small. So, the Term2 has the smallest contribution to the local change of deformation. It is evident that the advection will change the local deformation. As for the vertical velocity term, as mentioned above in section 2, in the case of three dimensions, vertical motion along the confluence zone will cause the upward transport of the moisture brought in by the horizontal deformation flow. It plays a role of adjusting the mass field and wind field, namely, the pressure and flow fields, and therefore leads to the change of local deformation.

7. Conclusions

In this paper, it has been shown that the total deformation is an invariant independent of the coordinate system it is expressed in. An idealized flow field was constructed to demonstrate the advection effect on 2D moisture fields by an essentially non-divergent and irrotational deformation flow that is similar to the flow patterns associated with typical heavy precipitation systems over eastern China, especially those associated with the mei-yu front. One heavy rainfall case was examined to explore the characteristics and role of total deformation before and during the heavy rainfall. Numerical simulation of the rainfall event was performed using the WRF model at a 27-km horizontal resolution and the model outputs were used for diagnostic analyses on the case.

Table 1. Correlation coefficients and RMS differences between individual terms in the total deformation equation and the sum of the terms for the July 2003 case.

Term	1	2	3	4	5
Correlation coefficient	0.523	−0.008	0.098	0.979	0.524
RMS (10^{-8} kg m^{-3} s^{-2})	2.976	3.581	3.309	0.051	2.310

It was found that before the onset of precipitation, the confluence effect associated with the deformation and the transport of moisture by such a flow sets up a favorable condition for heavy precipitation. During the precipitation period, both the location and orientation of the band of large total deformation and those of the confluent shear line are almost identical in the lower troposphere. The precipitation band is usually located slightly to the south of the shear line. The value of total deformation in the lower troposphere increases before and during the precipitation. The total deformation usually reaches its maximum value about 6 hours before the precipitation reaches its peak intensity. Therefore, the study on total deformation may be helpful for studying precipitation events, especially for the events associated with the mei-yu front and with deformation-dominant flow patterns.

To identify the major contributors to the change of total deformation, the total deformation equation was derived, in a similar way as the divergence and vorticity equations were. Calculations of individual terms in the equation showed that the pressure gradient term is the largest contributor to the local change of total deformation, whereas the vertical velocity term and advection terms also contribute to the change.

In this paper, only one heavy rainfall case was analyzed. To obtain more general conclusions, more cases should be examined, which is planned for the future. Data of higher temporal and spatial resolutions should be used to explore the relationship between the total deformation and the precipitation in more detail.

Acknowledgements. S. Gao and S. Yang were supported by the National Natural Science Foundation of China under Grant Nos. 40433007 and 40333028 and by the Olympic Project under Grant No. KACX1-02. M. Xue acknowledges the support from the Chinese Academy of Sciences (Grant No. 2004-2-7), which enabled the collaboration.

REFERENCES

Bluestein, H. B., 1977: Synoptic-scale deformation and tropical bands. *J. Atmos. Sci.*, **34**, 891–900.

Caracena, F., R. A. Maddox, L. R. Hoxit, and C. F. Chappell, 1979: Mesoanalysis of the big Thompson storm. *Mon. Wea. Rev.*, **107**, 1–17.

David, J. S., and J. L. Anderson, 2001: Is midlatitude convection an active or passive player in producing global circulation patterns? *J. Climate*, **14**, 2222–2237.

Davidson, N. E., K. Kurihara, T. Kato, G. Mills, and K. Puri, 1998: Dynamics and prediction of a mesoscale extreme rain event in the Baiu front over Kyushu, Japan. *Mon. Wea. Rev.*, **121**, 2005–2029.

Davies-Jones, R. P., 1984: The origin of updraft rotation in supercell storms. *J. Atmos. Sci.*, **41**, 2991–3006.

Droegemeier, K. K., S. M. Lazarus, and R. P. Davies-Jones, 1993: The influence of helicity on numerically simulated convective storms. *Mon. Wea. Rev.*, **121**, 2005–2029.

Dudhia, J., 1989: Numerical study of convection observed during the winter monsoon experiment using a mesoscale two-dimensional model. *J. Atmos. Sci.*, **46**, 3077–3107.

Etling, D., 1985: Some aspects of helicity in atmosphere flows. *Beitr. Phys. Atmos.*, **58**, 88–100.

Harasti, P. R., and R. List, 2005: Principal component analysis of Doppler radar data. Part I: Geometric connections between eigenvectors and the core region of atmosphere vorticies. *J. Atmos. Sci.*, **62**, 4027–4042.

Herbert, R., 1954: Rainfall and vorticity advection. *J. Atmos. Sci.*, **5**, 425–425.

Hong, S. Y., and H. L. Pan, 1996: Non-local boundary layer vertical diffusion in a medium-range forecast model. *Mon. Wea. Rev.*, **124**, 2322–2339.

Hoxit, L. R., J. M. Fritsch, and C. F. Chappell, 1978: Reply. *Mon. Wea. Rev.*, **106**, 1034–1034.

Kain, J. S., and J. M. Fritsch, 1990: A one-dimensional entraining/detraining plume model and its application in convective parameterization. *J. Atmos. Sci.*, **47**, 2784–2802.

Keyser, D., M. J. Pecnick, and M. A. Shapiro, 1986: Diagnosis of the role of vertical deformation in a two-dimensional primitive equation model of upper-level frontogenesis. *J. Atmos. Sci.*, **43**, 839–850.

Keyser, D., J. M. Reeder, and J. R. Reed, 1988: A generalization of Petterssen's frontogenesis function and its relation to the forcing of vertical motion. *Mon. Wea. Rev.*, **116**, 762–780.

Liebmann, B., J. A. Marengo, J. D. Glick, V. E. Kousky, I. C. Wainer, and O. Massamban, 1998: A comparison of rainfall, outgoing longwave radiation, and divergence over the Amazon Basin. *J. Climate*, **11**, 2892–2909.

Lilly, D. K., 1986a: The structure, energetics and propagation of rotation convective storms. Part I: Energy exchange with the mean flow. *J. Atmos. Sci.*, **43**,

113–125.

Lilly, D. K., 1986b: The structure, energetics and propagation of rotation convective storms. Part II: Helicity and storm stability. *J. Atmos. Sci.*, **43**, 126–140.

Lu, H., and S. Gao, 2003: On the helicity and the helicity equation. *Acta Ameteorologica Sinica*, **61**, 684–691. (in Chinese)

Maddox, R. A., L. R. Hoxit, C. F. Chappell, and F. Caracena, 1978: Comparison of meteorological aspects of the big Thompson and rapid city flash floods. *Mon. Wea. Rev.*, **106**, 375–389.

Maddox, R. A., F. Canova, and L. R. Hoxit, 1980a: Meteorological characteristics of flash flood events over the western United States. *Mon. Wea. Rev.*, **108**, 1866–1877.

Maddox, R. A., L. R. Hoxit, and C. F. Chappell, 1980b: A study of tornadic thunderstorm interactions with thermal boundaries. *Mon. Wea. Rev.*, **108**, 322–336.

Mlawer, E. J., S. J. Taubman, and P. D. Brown, 1997: Radiative transfer for inhomogeneous atmosphere: RRTM, a validated correlated-k model for the longwave. *J. Geophys. Res.*, **102**, 633–682.

Norbury, J., 2002: *Large-Scale Atmosphere-Ocean Dynamics*. Vol. I, Cambridge University Press, United Kingdom, 370pp.

Petterssen, S., 1956: *Weather Analysis and Forecasting*. Vol. I, 2nd ed., McGraw-Hill, New York, 428pp.

Rossby, C. G., 1937: On the mutual adjustment of pressure and velocity distribution in certain simple current systems, I. *J. Mar. Res.*, **1**, 15–28.

Rossby, C. G., 1938: On the mutual adjustment of pressure and velocity distribution in certain simple current systems, II. *J. Mar. Res.*, **2**, 239–263.

Stanley, L. U., and G. Michael, 1978a: The role of surface divergence and vorticity in the life cycle of convective rainfall. Part I: Observaton and analysis. *J. Atmos. Sci.*, **35**, 1047–1062.

Stanley, L. U., and G. Michael, 1978b: The role of surface divergence and vorticity in the life cycle of convective rainfall. Part II: Descriptive model. *J. Atmos. Sci.*, **35**, 1063–1069.

Walter, F., and A. J. Thorpe, 1979: An evaluation of theories of storm motion using observations of tropical convective systems. *Mon. Wea. Rev.*, **107**, 1306–1319.

Weisman, M. L., and J. B. Klemp, 1982: The dependence of numerically simulated convective storms on vertical wind shear and buoyancy. *Mon. Wea. Rev.*, **110**, 504–520.

Wicker, L. J., and J. S. William, 2002: Time-splitting methods for elastic models using forward time schemes. *Mon. Wea. Rev.*, **130**, 2088–2097.

Wiin-Nielsen, A., 1973: *Compendium of Meteorology*. Vol. I, WMO, 364pp.

Wu, R., and Z. Tan, 1989: Generalized vorticity and potential vorticity conversation law and application. *Acta Meteorologica Sinica*, **47**, 436–442. (in Chinese)

Yeh, T. C., 1957: On the formation of quasi-geostrohpic motion in the atmosphere. *J. Meteor. Soc. Japan* (75th anniversary volume), 130–137.

Yeh, T. C., and M. Li, 1982: On the characteristics of scales of the atmospheric motions. *J. Meteor. Soc. Japan*, **60**, 16–23.

Zeng, Q., 1963a: The effect of original disturbance structure on adaptation and the application of observed wind field. *Acta Meteorologica Sinica*, **33**, 37–50. (in Chinese)

Zeng, Q., 1963b: The adaptation and development in atmosphere. I. *Acta Meteorologica Sinica*, **35**, 163–174. (in Chinese)

Zeng, Q., 1963c: The adaptation and development in atmosphere. II. *Acta Meteorologica Sinica*, **35**, 281–189. (in Chinese)